
G-Net: A Deep Learning Approach to G-computation for Counterfactual Outcome Prediction Under Dynamic Treatment Regimes

Rui Li^{*1}, Zach Shahn^{*2,3}, Jun Li¹, Mingyu Lu¹, Prithwish Chakraborty^{2,3},
Daby Sow^{2,3}, Mohamed Ghalwash^{2,3}, Li-wei Lehman¹

¹Massachusetts Institute of Technology

²IBM Research, ³MIT-IBM Watson AI Lab

Abstract

Counterfactual prediction is a fundamental task in decision-making. G-computation is a method for estimating expected counterfactual outcomes under dynamic time-varying treatment strategies. Existing G-computation implementations have mostly employed classical regression models with limited capacity to capture complex temporal and nonlinear dependence structures. This paper introduces G-Net, a novel sequential deep learning framework for G-computation that can handle complex time series data while imposing minimal modeling assumptions and provide estimates of individual or population-level time-varying treatment effects. We evaluate alternative G-Net implementations using realistically complex temporal simulated data obtained from CVSim, a mechanistic model of the cardiovascular system.

1 Introduction

Counterfactual prediction is a fundamental task in decision-making. It entails the estimation of expected future trajectories of variables of interest under alternative courses of action (or *treatment strategies*) given observed history. Treatment strategies of interest are usually *time varying* (meaning they comprise decisions at multiple time points) and *dynamic* (meaning the treatment decision at each time point is a function of history up to that time point).

As an example, consider the problem of fluid administration in Intensive Care Units (ICUs) [1]. It is frequently necessary for physicians to adopt strategies that administer large volumes of fluids to increase blood pressure

and promote blood perfusion through organs in septic patients. However, such strategies can lead to fluid overload, which can have serious adverse downstream effects such as pulmonary edema. Fluid administration strategies are time varying and dynamic because at each time point physicians decide the volume of fluid to administer based on observed patient history (e.g. blood pressure and volume of fluid already administered) up to that time point. To aid in the choice between alternative dynamic fluid administration strategies, it would be desirable to obtain counterfactual predictions of a patient’s probability of developing fluid overload (and other outcomes of interest) were they to follow each alternative strategy going forward given their observed covariate history up to the current time.

Counterfactual prediction is an inherently *causal* task in that it must account for the causal effects of following different treatment strategies. When treatment strategies of interest are time-varying, so-called “g-methods” [2, 3] are required to estimate their effects. G-methods include g-computation [4–6], structural nested models [7, 8], and marginal structural models [9, 10]. Of these methods, g-computation is best suited for estimating effects of general dynamic treatment strategies conditional on high dimensional patient histories [11].

G-computation works by estimating the conditional distribution of relevant covariates given covariate and treatment history at each time point, then producing Monte Carlo estimates of counterfactual outcomes by simulating forward patient trajectories under treatment strategies of interest. Regression model(s) for the covariates and outcomes at each time point conditional on observed history are a critical component of this method. While any regression models could in theory be input to the G-computation algorithm, most existing G-computation implementations have employed simple regression models with limited capacity to capture complex temporal and nonlinear dependence structures. In recent years, sequential deep learning methods such as Recurrent Neural Networks (RNNs) have achieved state of the art performance in predictive modeling of complex time series data while imposing minimal

* Co-first authors. Correspondence to: Li-wei Lehman (lilehman@mit.edu), Zach Shahn (zach.shahn@ibm.com).
Copyright ©2020 by the authors.

modeling assumptions. In this paper, we propose G-Net, a sequential deep learning framework for G-computation. G-Net admits the use of recurrent networks such as LSTMs to model covariates in a manner suitable for G-computation. The G-Net framework is flexible and allows for various configurations depending on the problem at hand. To the best of our knowledge, this is the first work to investigate a RNN based approach to G-computation.

Unfortunately, it is impossible to reliably evaluate counterfactual predictions on real data, since only the outcomes corresponding to treatment strategies that were actually followed can be observed. Consequently, to explore and evaluate various implementations of G-Net, we used simulated data in which counterfactual ground truth can be known. We used CVSim [12], a well established mechanistic model of the cardiovascular system, to estimate counterfactual simulated patient trajectories under various fluid and vasopressor administration strategies. These experiments provide a template for causal model evaluation using complex and physiologically realistic simulated longitudinal data.

2 Related Work

Several recent works have proposed a deep learning framework for counterfactual prediction from observational data, including [13–15]. However, these works have mostly focused on learning point exposure as opposed to time-varying treatment effects, which are the focus of this paper.

G-computation for estimating time-varying treatment effects was first proposed by Robins [4]. Illustrative applications of the general approach are provided in [6, 16], and summaries of g-computation (and other “g-methods” for estimating time-varying treatment effects) can be found in [2, 3]. The g-computation algorithm takes arbitrary regression models as inputs. While most applications (e.g. [6, 16]) have thus far employed classical generalized linear models, there is no conceptual barrier to using more complex machine learning regression models. RNNs, and in particular LSTMs, have achieved state of the art performance on a wide variety of time series regression tasks, including healthcare related tasks [17–19]. However, despite the popularity and success of RNNs for time series regression, we have not seen in the literature any “deep” implementation of g-computation.

Recently, Lim et al. [20] plugged RNN regression models into history adjusted marginal structural models (MSM) [21] to make counterfactual predictions. However, these MSMs can only make counterfactual predictions under *static* time-varying treatment strategies that do not depend on recent covariate history. For example, a history adjusted MSM [20] could estimate the probability of fluid overload given patient history under the (static) treatment strategy “give 1 liter fluid each hour for the next 3 hours”, but it could not estimate the probability of fluid overload

given patient history under the (dynamic) treatment strategy “each hour for the next 3 hours, if blood pressure is less than 65 then give 1 liter fluids, otherwise give 0 liters”. History adjusted MSMs cannot estimate effects of time-varying treatment strategies that respond to changes in the patient’s health history, but g-computation can. Further, g-computation is able to straightforwardly estimate the *distribution* of a counterfactual outcome under a time-varying treatment strategy. This is not straightforward to do with history adjusted MSMs.

Schulam and Saria [22] propose Counterfactual Gaussian Processes, an implementation of continuous time g-computation, and like us apply their method to ICU data. They only consider static time-varying treatment strategies, though it appears that their method might straightforwardly be extended to handle dynamic strategies as well. An advantage of Gaussian processes is interpretable uncertainty quantification. However, GPs are intractable for large datasets since they have time complexity of $O(N^3)$, where N is the number of observations [23]. Sparse GPs, which introduce M inducing points, have at least $O(M^2N)$ [23] time complexity. RNNs are more scalable. Recurrent dropout can also be employed in RNN based implementations to produce uncertainty estimates that approximate posterior distributions from a Gaussian process [24].

3 G-computation for counterfactual prediction

Our goal is to predict patient outcomes under various future treatment strategies given observed patient histories. Let:

- $t \in \{0, \dots, K\}$ denote time, assumed discrete, with K being the end of followup;
- A_t denote the observed treatment action at time t ;
- Y_t denote the observed value of the outcome at time t ;
- L_t denote a vector of covariates at time t that may influence treatment decisions or be associated with the outcome;
- \bar{X}_t denote the history X_0, \dots, X_t and \underline{X}_t denote the future X_t, \dots, X_K for arbitrary time varying variable X .

At each time point, we assume the causal ordering (L_t, A_t, Y_t) . Let $H_t \equiv (\bar{L}_t, \bar{A}_{t-1})$ denote patient history preceding treatment at time t . A dynamic treatment strategy g is a collection of functions $\{g_0, \dots, g_K\}$, one per time point, such that g_t maps H_t onto a treatment action at time t . A simple dynamic strategy for fluid volume might be $g_t(H_t) = .5 \times \mathbf{1}\{bp_t < 65\}$, i.e. give .5 liters of fluid if mean arterial blood pressure is less than 65 at time t .

Let $Y_t(g)$ denote the counterfactual outcome that would be observed at time t had, possibly contrary to fact, treatment strategy g been followed from baseline [4]. Further, let $Y_t(\bar{A}_{m-1}, \underline{g}_m)$ with $t \geq m$ denote the counterfactual

outcome that would be observed had the patient received their observed treatments \bar{A}_{m-1} through time $m - 1$ then followed strategy g from time m onward.

In counterfactual point prediction, our goal is to estimate expected counterfactual patient outcome trajectories

$$\{E[Y_t(\bar{A}_{m-1}, \underline{g}_m) | H_m], t \geq m\} \quad (1)$$

given observed patient history through time m for any m and any specified treatment strategy g . We might also be interested in estimating the counterfactual outcome distributions at future time points

$$\{p(Y_t(\bar{A}_{m-1}, \underline{g}_m) | H_m), t \geq m\}. \quad (2)$$

If we do not condition on anything in H_m , then (1) is an expectation (and (2) a distribution) over the full population. If we condition on a small subset of variables contained in patient history, then (1) is an expectation (and (2) a distribution) over a sub-population. If we condition on all elements of a patient history, then (1) is still technically only an expectation (and (2) a distribution) over a hypothetical sub-population with the exact patient history conditioned on, but in this case (1) and (2) practically amount to what is usually meant by personalized prediction.

Under the below standard assumptions, we can estimate (1) and (2) through g-computation [4].

1. **Consistency:** $\bar{Y}_K(\bar{A}_K) = \bar{Y}_K$
2. **Sequential Exchangeability:** $\underline{Y}_t \perp\!\!\!\perp A_t | H_t \quad \forall t$
3. **Positivity:** $P(A_t = g_t(H_t)) > 0 \quad \forall \{H_t : P(H_t) > 0\}$

Assumption 1 states that the observed outcome is equal to the counterfactual outcome corresponding to the observed treatment. Assumption 2 states that there is no unobserved confounding of treatment at any time and any future outcome. Assumption 2 would hold, for example, under the conditions depicted in Figure 1. Positivity states that the counterfactual treatment strategy of interest has some non-zero probability of actually being followed. Under the assumption that we specify certain predictive models correctly such that their predictions extrapolate to parts of a joint distribution that they were not trained on, positivity is not strictly necessary.

Under assumptions 1-3, for $t = m$ we have simply that

$$p(Y_m(\bar{A}_{m-1}, g_m) | H_m) = p(Y_m | H_m, A_m = g_m(H_m)), \quad (3)$$

i.e. the conditional distribution of the counterfactual is simply the conditional distribution of the observed outcome given patient history and given that treatment follows the strategy of interest. For $t > m$, things are slightly more complex because we need to adjust for time-varying confounding. With $X_{i:j} = X_i, \dots, X_j$ for any random variable X , under Assumptions 1-3 the g-formula yields

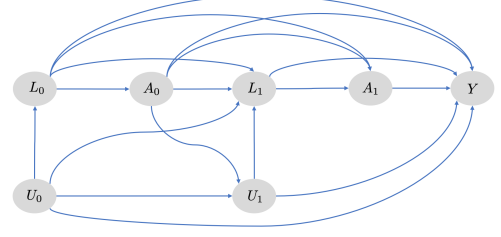


Figure 1: A causal DAG representing a data generating process in which Assumption 2 (sequential exchangeability) holds. This DAG represents a simple two time step process where the outcome is measured only after the final time step. However, its salient property is that all variables influencing treatment (i.e. with arrows directly into treatment) and associated with future outcomes are measured.

$$\begin{aligned} p(Y_t(\bar{A}_{m-1}, \underline{g}_m) = y | H_m) \\ &= \int_{l_{m+1:t}} p(Y_t = y | H_m, L_{m+1:t} = l_{m+1:t}, A_{m:t} = g(H_{m:t})) \\ &\quad \times \prod_{j=m+1}^t p(L_j = l_j | H_m, L_{m+1:j-1} = l_{m+1:j-1}, \\ &\quad \quad \quad A_{m,j-1} = g(H_m, l_{m+1:j-1})). \end{aligned} \quad (4)$$

It is not generally possible to compute this integral in closed form, but it could be approximated through Monte-Carlo simulation. We repeat the recursive process shown in Algorithm 1 M times. (Here the outcome Y_t is without loss of generality deemed to be a variable in the vector L_{t+1} .)

At the end of this process, we have M simulated draws of the counterfactual outcome for each time $t = \{m, \dots, K\}$. For each t , the empirical distribution of these draws constitutes a Monte-Carlo approximation of the counterfactual outcome distribution (2). The sample averages of the draws at each time t are an estimate of the conditional expectations (1) and can serve as point predictions for $Y_t(\bar{A}_{m-1}, \underline{g}_m)$ in a patient with history H_m .

Key to the g-computation algorithm is the ability to simulate from joint conditional distributions $p(L_t | \bar{L}_{t-1}, \bar{A}_{t-1})$ of the covariates given patient history at time t . Of course, in practice we do not have prior knowledge of these conditional distributions and need to estimate them from data. Most implementations use generalized linear regression models to estimate the conditional distributions of the covariates. Often, these models do not capture temporal dependencies present in the patient data. We propose the G-Net for this task.

4 G-Net Design

The proposed G-Net framework depicted in Figure 2 enables the use of sequential deep learning models to estimate conditional distributions $p(\bar{L}_t | \bar{L}_{t-1}, \bar{A}_{t-1})$ of covariates given history at each time point and perform the G-

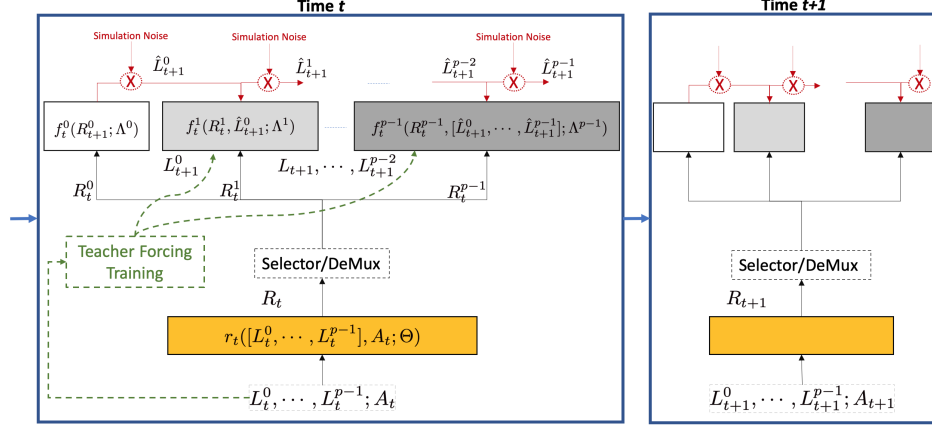


Figure 2: The G-Net: A flexible sequential deep learning framework for g-computation.

Algorithm 1: G-Computation (One simulation)

- 1 Set $a_m^* = g_m(H_m)$
 - 2 Simulate and record y_m^* from $p(Y_m|H_m, A_m = a_m^*)$
 - 3 Simulate l_{m+1}^* from $p(L_{m+1}|H_m, A_m = a_m^*)$
 - 4 Set $a_{m+1}^* = g_m(H_m, l_{m+1}^*, a_m^*)$
 - 5 Simulate and record y_{m+1}^* from $p(Y_{m+1}|H_m, L_{m+1} = l_{m+1}^*, A_m = a_m^*, A_{m+1} = a_{m+1}^*)$
 - 6 Simulate l_{m+2}^* from $p(L_{m+2}|H_m, L_{m+1} = l_{m+1}^*, A_m = a_m^*, A_{m+1} = a_{m+1}^*)$
 - 7 Continue simulations through time K
-

computation algorithm described in Algorithm 1 to simulate covariates under various treatment strategies. In this setting, without loss of generality, we set Y_t as one of the co-variables in L for notational simplicity.

Let L_t^0, \dots, L_t^{p-1} denote p components of the vector L_t , where each component L_t^j could be multivariate. We impose an arbitrary ordering $L_1^0, L_1^1, L_1^2, \dots, L_1^{p-1}, A_1, \dots, L_K^0, L_K^1, L_K^2, \dots, L_K^{p-1}, A_K$ and estimate the conditional distributions of each L_t^j given all variables preceding it in this ordering. At simulation time, we exploit the basic probability identity

$$p(L_t|\bar{L}_{t-1}, \bar{A}_{t-1}) = p(L_t^0|\bar{L}_{t-1}, \bar{A}_{t-1}) \times p(L_t^1|L_t^0, \bar{L}_{t-1}, \bar{A}_{t-1}) \times \dots \times p(L_t^{p-1}|L_t^0, \dots, L_t^{p-2}, \bar{L}_{t-1}, \bar{A}_{t-1})$$

to simulate from $p(L_t|\bar{L}_{t-1}, \bar{A}_{t-1})$ by sequentially simulating each L_t^j from $p(L_t^j|L_t^0, \dots, L_t^{j-1}, \bar{L}_{t-1}, \bar{A}_{t-1})$. There are at least two reasons to allow for subdivision of the covariates. First, if covariates are of different types (e.g. continuous, categorical, count, etc.), it is difficult to simultaneously simulate from their joint distribution. Second, customizing models for each covariate component can potentially lead to better performance. Figure 2 illustrates this decomposition where at each time point the components are depicted via ordered (grey shaded) boxes that are responsible for the estimation of the various terms needed to

compute the conditional distributions. One could set $p = 1$ and model all covariates simultaneously or at the other extreme set p to be the total number of variables.

The sequential model used in G-Net provides us with estimates of the conditional expectations $E[L_t^j|\bar{L}_{t-1}, L_t^0, \dots, L_t^{j-1}, \bar{A}_{t-1}]$ for all t and j . To simulate from $p(L_t^j|\bar{L}_{t-1}, L_t^0, \dots, L_t^{j-1}, \bar{A}_{t-1})$, we proceed as follows. If L_t^j is multinomial, its conditional expectation defines its conditional density. If L_t^j has a continuous density, there are various approaches we might take to simulate from its conditional distribution. Without making parametric assumptions, we could simulate from

$$L_t^j|L_t^0, \dots, L_t^{j-1}, \bar{L}_{t-1}, \bar{A}_{t-1} \sim \hat{E}[L_t^j|L_t^0, \dots, L_t^{j-1}, \bar{L}_{t-1}, \bar{A}_{t-1}] + \epsilon_t^j \quad (5)$$

where ϵ_t^j is a draw from the empirical distribution of the residuals $L_t^j - \hat{L}_t^j$ in a holdout set not used to fit the model parameters used to generate \hat{L}_t^j as an estimate of $E[L_t^j|L_t^0, \dots, L_t^{j-1}, \bar{L}_{t-1}, \bar{A}_{t-1}]$. This method makes the simplifying assumption that the covariate error distribution does not depend on patient history. This is the approach we take in the experiments in this paper, and is depicted in the simulation noise nodes at the top of Figure 2. Alternatively, we might specify a parametric distribution for $L_t^j - E[L_t^j|L_t^0, \dots, L_t^{j-1}, \bar{L}_{t-1}, \bar{A}_{t-1}]$, e.g. a Gaussian, and directly estimate its parameters by maximum likelihood.

To obtain the estimates for the conditional distribution of covariates, G-Net admits sequential modeling of patients' data using the group decomposition and arbitrary ordering outlined before. As shown in the yellow boxes in Figure 2, at each time t , a representation R_t of the patient history can be computed as

$$R_t = r_t(\bar{L}_t, \bar{A}_t; \Theta) \quad (6)$$

where Θ represents model parameters learned during training. In its simplest form, r_t may just be an identity func-

tion passing the covariates. In other configurations (e.g. using the selector in Figure 2), r_t can be used to provide abstractions of histories using sequential learning architectures such as RNN. This formulation of r_t allows for a great deal of flexibility in how information is shared across variables and time.

Estimates from each of the p covariate groups can then be obtained, as shown in Figure 2, by successive estimation of conditional expectations of covariates. Specifically, the conditional expectation of each L_{t+1}^j , $0 \leq j < p$ given the representation of patient history R_t and the other variables from time $t + 1$ that precede it in the arbitrary predefined ordering is estimated by the functions f_t^j . The complete sequence can be given as follows:

$$\begin{aligned}
 L_{t+1}^0 &= f_t^0(R_t; \Lambda_0) \\
 L_{t+1}^1 &= f_t^1(R_t, L_{t+1}^0; \Lambda_1) \\
 &\dots \\
 L_{t+1}^j &= f_t^j(R_t, [L_{t+1}^1, \dots, L_{t+1}^{j-1}]; \Lambda_j) \\
 &\dots
 \end{aligned} \tag{7}$$

where, each of the f_t^j represents the specialized estimation function for group j and Λ_j are the learnable parameters for the same. Depending on modeling choices, f_t^j can be sequential models specialized for group j or models focusing only on the time step t (e.g. linear models).

Given G-Net parameters, the distribution of the Monte Carlo simulations produced by G-computation Algorithm 1 constitute an estimate of uncertainty about a counterfactual prediction. But this estimate ignores uncertainty about the G-Net parameter estimates themselves. One way to incorporate such model uncertainty would be to fit a Bayesian model and, before each Monte Carlo trajectory simulation in G-computation, draw new network parameters from their posterior distribution. These Monte Carlo draws would be from the posterior predictive distribution of the counterfactual outcome. Bayesian deep learning can be prohibitively computationally intensive, but can be approximated through dropout [24]. First, we fit the RNN component of the G-Net using recurrent dropout, with dropout masks at each layer held constant across time as described in [24]. Let M denote a dropout mask constant across time for each layer of the RNN, $\hat{\Theta}(M)$ denote estimated RNN parameters with mask M applied, and p_M denote the distribution from which M was sampled during training. Then, during g-computation, we add *step 0* to the beginning of Algorithm 1 before each simulation:

Step 0 (dropout) : Sample $D^* \sim p_D$

and compute all simulations plugging $\hat{E}_{\Theta(D)}[L_t^j | L_t^1, \dots, L_t^{j-1}, \bar{L}_{t-1}, \bar{A}_{t-1}]$ into (5). Then draws of $\hat{\Theta}(D)$ are from an approximation to the posterior distribution of Θ under a particular Gaussian Process prior.

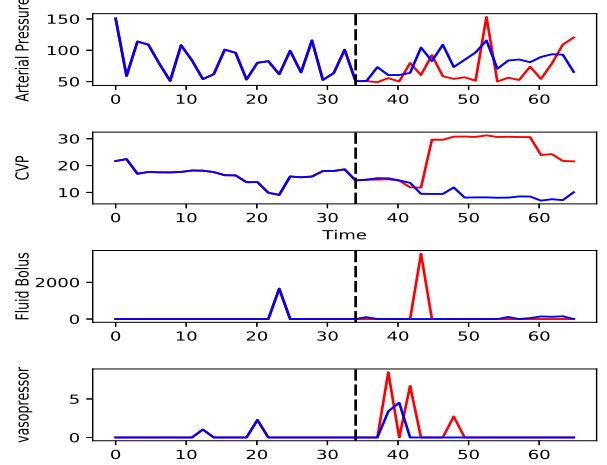


Figure 3: Covariates trajectories for the same patient (i.e. the same random seed) under two different treatments g_o (blue) and g_c (red). After the treatment strategies diverge at middle of trajectory, $t = 34$ (black dashed line), g_c delivers a large fluid dose while g_o does not, temporarily pushing AP and CVP higher under the g_c regime than the g_o regime.

Therefore, the Monte Carlo simulations obtained from g-computation incorporating dropout (i.e. adding step 0 as above) approximate draws from the posterior predictive distribution of the counterfactual outcome.

The parameters, Θ and Λ , are learned by optimizing a loss function forcing the G-Net to accurately estimate covariates L_t at each time point t using standard gradient descent techniques. It is to be noted that it is necessary to use teacher-forcing (using observed values of L_{t+t}^j as arguments to f_t in equation) to obtain unbiased estimates of f_t , as shown in Figure 2.

5 Simulation Experiments Using CVSim

To evaluate counterfactual predictions, it is necessary to use simulated data in which counterfactual ground truth for outcomes under alternative treatment strategies is known. To this end, we performed experiments on data generated by CVSim [25], a program that simulates the dynamics of the human cardiovascular system.

Data Generation: We generated an ‘observational’ dataset D_o under treatment regime g_o and two ‘counterfactual’ datasets D_{c1} and D_{c2} under treatment regimes g_{c1} and g_{c2} . The data generating processes producing D_o and D_{c_j} were the same except for the treatment assignment rules. For each j , g_{c_j} was identical to g_o for the first $m - 1$ simulation time steps before diverging to a different treatment rule for time steps m to K as illustrated in Figure 3.

A CVSim 6-compartment circulatory model takes as inputs 28 variables that together govern a hemodynamic system. It then deterministically simulates forward in time a set of

25 output variables according to a collection of differential equations (parameterized by the input variables) modeling hemodynamics. Important variables in CVSim include arterial pressure (AP), central venous pressure (CVP), total blood volume (TBV), and total peripheral resistance (TPR). In real patients, physicians observe AP and CVP and seek to keep them above a clinically safe threshold. They do this by intervening on TBV (through fluid administration) and TPR (through vasopressors).

We defined simulated treatment interventions that were designed to mimic the impact of fluids and vasopressors. These simulated interventions alter the natural course of the simulation by increasing either TBV (in the case of the simulated fluids intervention) or TPR (in the case of the simulated vasopressor intervention). We generated patients by randomly initiating baseline inputs (which we hid from our G-Nets to make this a stochastic modeling problem) within plausible physiologic ranges, then using CVSim to simulate covariates forward, intervening according to the relevant treatment strategy at each timestep. Full details of the simulation process can be found in the Appendix.

Under (stochastic) observational treatment strategy g_o , the probability of receiving a non-zero vasopressor or fluid dose at a given time increases as MAP and CVP decrease according to a logistic regression function. Given that a dose is non-zero, the exact amount is drawn from a normal distribution with mean inversely proportional to MAP and CVP. Since all drivers of treatment under g_o are observed in our data, the sequential exchangeability assumption holds and g-computation may be validly applied.

g_{c1} is similar to g_o , except it is a deterministic treatment strategy and the functions linking treatment and dose to covariates have different coefficients. Under g_{c2} , treatment is always withheld. Again, details are in the Appendix.

Experiment Setup: We set ourselves the task of training a G-Net on D_o and using it to predict the trajectories of patients in D_{cj} for time steps m to K for each j . This setup is designed to evaluate the performance of a G-Net in a situation in which we observe data from past patients (D_o) who received usual care (g_o) for K timesteps and would like to predict how a new patient who has been observed for m timesteps would fare were they to follow a different treatment strategy of interest (g_{cj}) for timesteps m to K . This is a standard use case for counterfactual prediction. D_{cj} provides ground truth for a collection of patients whose trajectories follow just the path we are interested in predicting. Thus, by aggregating predictive performance metrics across simulated patients in D_{cj} we generate measures of the population level performance of our G-Net at the counterfactual prediction task for which it was intended.

As shown in Table 1, we explore two specific criteria: (a) using sequential vs. Identity functions for r_t and (b) using sequential models of entire patient history vs. linear models

Table 1: Experimental Model Setup Grid: Each cell summarizes the instantiations: $M1(Linear)$, $M2(LSTM)$, $M3(LSTM)$, and $M4(LSTM)$, of G-Net used in our experiments.

	With pass thru r_t	With sequential r_t
$f_i:LR$	$M1(Linear)$	$M2(LSTM)$
	<ul style="list-style-type: none"> • r_t: identity • $p = 2$ • (f_0, f_1): linear layers. 	<ul style="list-style-type: none"> • r_t: LSTM • $p = 2$ • (f_0, f_1): linear layers.
$f_i:RNN$	$M3(LSTM)$	$M4(LSTM)$
	<ul style="list-style-type: none"> • r_t: identity • $p = 2$ • (f_0, f_1): LSTMs. 	<ul style="list-style-type: none"> • r_t: LSTM • $p = 2$ • (f_0, f_1): LSTMs

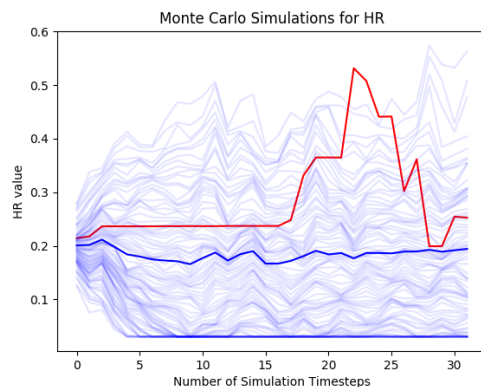


Figure 4: 100 G-Net simulated trajectories (blue) and ground truth (red) for one patient under g_{c1} .

focusing only on current time point for f_t . This provides us 4 different implementations of G-Net.

The best parameters for each model found from grid search are as follows. For $M2(LSTM)$ the hidden dimension for the representational LSTM is 30, the hidden dimension for the categorical LSTM is 5, the hidden dimension for the continuous LSTM is 30, and the learning rate is .001. For $M3(LSTM)$, the hidden dimension for the categorical LSTM is 10, the hidden dimension for the continuous LSTM is 75, and the learning rate is .005. For $M4(LSTM)$, the hidden dimension for the representational LSTM is 30, the hidden dimension for the categorical LSTM is 5, the hidden dimension for the continuous LSTM is 30, and the learning rate is .001. For all models, the batch size used was 64. These parameters were the ones used to achieve the results presented in the experiments and results section.

Evaluation: We evaluate the accuracy (Mean Squared Error - MSE) and calibration of the counterfactual simulations generated by our G-Nets as follows. Say D_{cj} comprises N_c trajectories of random variable $(\bar{L}_K^{cj}, \bar{A}_K^{cj})$. Given observed history $H_{mi}^{cj} = (\bar{L}_{mi}^{cj}, \bar{A}_{m-1i}^{cj})$ for patient i from

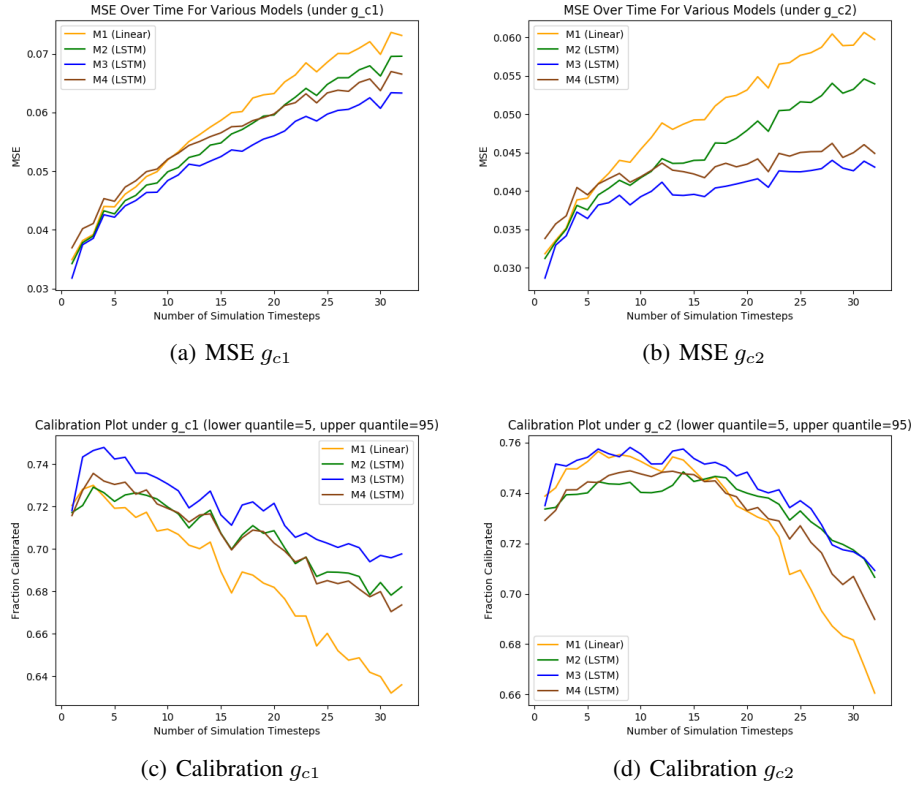


Figure 5: Performance of various models: MSE and calibration over time for g_{c1} and g_{c2}

D_{cj} , a G-Net G fit to D_o produces M (in our experiments, 100) simulations of the counterfactual covariate trajectory $\{\tilde{L}_{ti}^{cj}(H_{mi}^{cj}, G, k) : t \in m : K; k \in 1 : M\}$. These simulated trajectories are the light blue lines in Figure 4.

The G-Net’s point prediction of L_{ti} is its estimate of $E[L_t(g_{cj})|H_m = H_{mi}]$, i.e. the average of the M simulations $\hat{L}_{ti}(G) \equiv \frac{1}{M} \sum_{k=1}^M \tilde{L}_{ti}^c(H_{mi}^c, G, k)$. This is the dark blue line in Figure 4.

If L_t has dimension d , we compute the MSE of counterfactual predictions by a G-Net G in the dataset D_c as $\frac{1}{N_c(K-m)d} \sum_{i=1}^{N_c} \sum_{t=m}^K \sum_{h=1}^d (L_{ti}^{h,CF} - \hat{L}_{ti}^{h,CF}(G))^2$.

We assess the calibration of a G-Net G as follows. Given lower and upper quantiles α_{low} and α_{high} , the calibration measures the frequency with which the actual counterfactual covariate $L_{ti}^{h,cj}$ is between the α_{low} and α_{high} quantiles of the M simulations $\{\tilde{L}_{ti}^{h,cj}(H_{mi}^{cj}, G, k) : k \in 1 : M\}$. If this frequency is approximately $\alpha_{high} - \alpha_{low}$, then G is well calibrated.

Experiments/Results: Using CVSim, we generated a total of 10,000 trajectories in D_o ($N_o = 10,000$), of which 80% were used for training, and the remaining 20% for validation. For testing, we generated 500 observations in the D_{cj} datasets ($N_c = 500$). We included a total of 18 output variables (including all variables influencing treatment as-

signed under g_o) from CVSim to construct D_o and D_{cj} ; each trajectory is of length 64 time steps ($d=18, K=64$). In each D_{cj} , the switching time point m from g_o to g_c is fixed at 34 for all trajectories ($m = 34$).

We fit the four models described in Table 1 to the training portion of D_o (80%), and used the remaining portion as validation to tune our model hyperparameters. Next, given observed covariate history through 34 time steps and treatment history through 33 time steps of each trajectory in each D_{cj} , we computed the MSE and calibration of the G-Nets’ counterfactual predictions for time steps 34 to 64.

Figure 5 (a) and (b) illustrates the performance of the various G-Net architectures in terms of MSE over time. Overall, for this experiment we found M3 (Identity function for r_t and LSTM for the f_i functions), performed best over both treatment strategies. Also, a comparative analysis of M1 vs M3 (both with Identity representation function for r_t) and M2 vs M4 (both with LSTM representation functions for r_t) showed that G-Net provide better estimates of conditional distributions by admitting sequential prediction models focusing on the entire patient history compared to prediction models focusing on a single time point.

Figure 5 (c) and (d) depicts calibration for the candidate models. All of the calibration coverage rates are below the nominal levels (they should be .5), though the RNN based

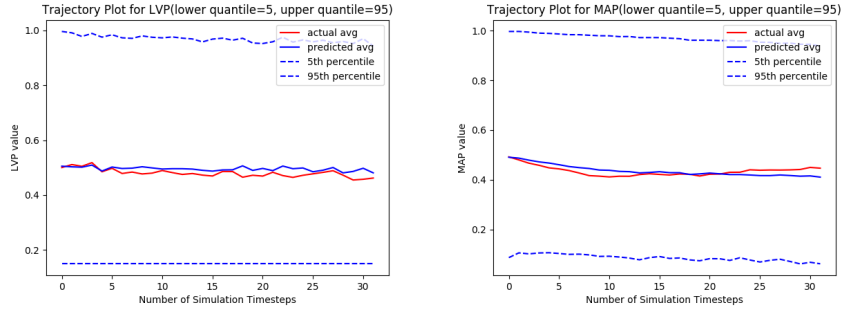


Figure 6: Estimated (G-Net $M3$ in Table 1) and actual population average trajectories under g_{c1} for select variables.

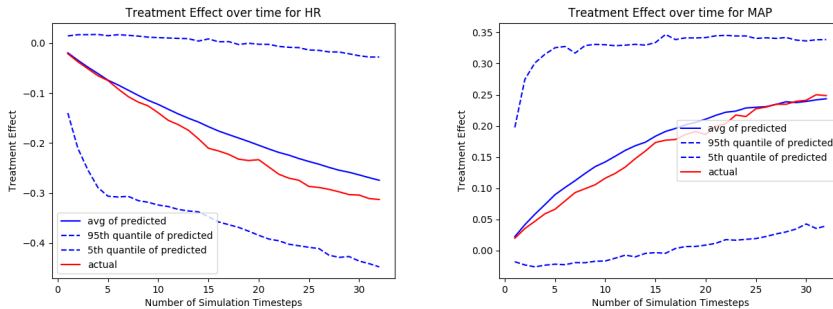


Figure 7: Treatment Effect for Selected Variables

G-Nets again perform better than the linear model implementation. This is in part because the counterfactual predictive density estimates in these experiments do not take into account uncertainty about model parameter estimates, which could be addressed with dropout as discussed in Section 4.

The G-Net can also be used to estimate population average counterfactual outcomes and treatment effects, quantities sometimes more relevant to policy decisions than individual level counterfactual predictions. Figure 6 displays G-Net ($M3$ from Table 1) estimates and true values of population average trajectories for select variables under g_{c1} . Figure 7 shows estimates and true values of the population average treatment effect of following g_{c1} as opposed to g_{c2} on select variables. We see that the G-Net does a good job of estimating these population level quantities of interest.

6 Discussion and Future Work

In the G-Net we have introduced a novel and flexible framework for counterfactual prediction under dynamic treatment strategies through G-computation using sequential deep learning models. We have illustrated several implementations of the G-Net in a realistically complex simulation setting where we had access to ground truth counterfactual outcomes. In particular, we considered alternative approaches to representation learning that either share

representations of patient history across predictive tasks or keep them separate. In the particular implementation we considered, shared representations seemed to aid simple linear classifiers but harm LSTMs.

The G-Net framework’s flexibility means that there are many other alternative implementations to explore. For example, we might consider alternative architectures for representing patient history, such as attention mechanisms or memory networks.

Another direction of future work is incorporation of prior causal knowledge. For example, if it is known which variables are confounders and which merely predictive of the outcome, we might include weights in the loss function emphasizing faithful representation and prediction of confounding variables compared to non-confounders.

References

- [1] Simon Finfer, John Myburgh, and Rinaldo Bellomo. Intravenous fluid therapy in critically ill adults. *Nature Reviews Nephrology*, 14(9):541, 2018.
- [2] Miguel Hernan and James Robins. *Causal Inference*. Chapman and Hall, Forthcoming.
- [3] James Robins and Miguel Hernan. Estimation of the causal effects of time varying exposures. In Garrett Fitzmaurice, Marie Davidian, Geert Verbeke, and

-
- Geert Molenberghs, editors, *Longitudinal Data Analysis*, pages 553–599. Chapman and Hall, 2009.
- [4] James Robins. A new approach to causal inference in mortality studies with a sustained exposure period: application to control of the healthy worker survivor effect. *Mathematical Modelling*, 1986.
- [5] James Robins. A graphical approach to the identification and estimation of causal parameters in mortality studies with sustained exposure periods. *Journal of Chronic Diseases*, 1987.
- [6] Sarah Taubman, James Robins, Murray Mittleman, and Miguel Hernan. Intervening on risk factors for coronary heart disease: An application of the parametric g-formula. *International journal of epidemiology*, 2009.
- [7] James Robins. Correcting for non-compliance in randomized trials using structural nested mean models. *Communications in Statistics-Theory and Methods*, 1994.
- [8] Stijn Vansteelandt and Marshall Joffe. Structural nested models and g-estimation: The partially realized promise. *Statistical Science*, 2014.
- [9] James Robins, Miguel Hernan, and Babette Brumback. Marginal structural models and causal inference in epidemiology. *Epidemiology*, 2000.
- [10] Liliana Orellana, James Robins, and Andrea Rotnitzky. Dynamic regime marginal structural mean models for estimation of optimal dynamic treatment regimes. *The international journal of biostatistics*, 2008.
- [11] James Robins. A new approach to causal inference in mortality studies with a sustained exposure period: application to control of the healthy worker survivor effect. *Mathematical modelling*, 7(9-12):1393–1512, 1986.
- [12] Thomas Heldt, Ramakrishna Mukkamala, George B Moody, and Roger G Mark. Cvsim: an open-source cardiovascular simulator for teaching and research. *The open pacing, electrophysiology & therapy journal*, 3:45, 2010.
- [13] Onur Atan, James Jordan, and Mihaela van der Schaar. Deep-treat: Learning optimal personalized treatments from observational data using neural networks. In *Proceedings of AAAI*, 2018.
- [14] M Ahmed Alaa, Michael Weisz, and Mihaela van der Schaar. Deep counterfactual networks with propensity-dropout. In *Proceedings of the 34th International Conference on Machine Learning (ICML)*, 2017.
- [15] Jinsung Yoon, James Jordan, and Mihaela van der Schaar. Ganite: Estimation of individualized treatment effects using generative adversarial nets. In *ICLR.*, 2018.
- [16] Jessica Young, Lauren Cain, James Robins, Eilis O’Reilly, and Miguel Hernan. Comparative effectiveness of dynamic treatment regimes: An application of the parametric g-formula. *Statistics in biosciences*, 2011.
- [17] Nenad Tomašev, Xavier Glorot, Jack W Rae, Michal Zielinski, Harry Askham, Andre Saraiva, Anne Mottram, Clemens Meyer, Suman Ravuri, Ivan Protsyuk, et al. A clinically applicable approach to continuous prediction of future acute kidney injury. *Nature*, 572(7767):116, 2019.
- [18] Cao Xiao, Edward Choi, and Jimeng Sun. Opportunities and challenges in developing deep learning models using electronic health records data: a systematic review. *Journal of the American Medical Informatics Association*, 25(10):1419–1428, 06 2018.
- [19] Edward Choi, Mohammad Taha Bahadori, Jimeng Sun, Joshua Kulas, Andy Schuetz, and Walter Stewart. Retain: An interpretable predictive model for healthcare using reverse time attention mechanism. In D. D. Lee, M. Sugiyama, U. V. Luxburg, I. Guyon, and R. Garnett, editors, *Advances in Neural Information Processing Systems 29*, pages 3504–3512. Curran Associates, Inc., 2016.
- [20] Bryan Lim, Ahmed Alaa, and Mihaela van der Schaar. Forecasting treatment responses over time using recurrent marginal structural networks. In *Neural Information Processing Systems (NIPS).*, 2018.
- [21] Mark van der Laan, Maya Petersen, and Marshall Joffe. History-adjusted marginal structural models and statically-optimal dynamic treatment regimens. *The international journal of biostatistics*, 2005.
- [22] Peter Schulam and Suchi Saria. Reliable decision support using counterfactual models. In *Neural Information Processing Systems (NIPS).*, 2017.
- [23] Michalis Titsias. Variational learning of inducing variables in sparse gaussian processes. In *International Conference on Artificial Intelligence and Statistics*, 2009.
- [24] Yarin Gal and Zoubin Ghahramani. A theoretically grounded application of dropout in recurrent neural networks. In *Advances in Neural Information Processing Systems*, 2016.
- [25] T Heldt, R Mukkamala, GB Moody, and RG Mark. CVSim: An open-source cardiovascular simulator for teaching and research. *Open Pacing, Electrophysiol & Ther J*, 3:45–54, 2010.
- [26] Andrew Rhodes, Waleed Evans, Laura E. and Alhazzani, Mitchell M. Levy, Massimo Antonelli, Ricard Ferrer, Anand Kumar, Jonathan E. Sevransky,

Charles L. Sprung, Mark E. Nunnally, et al. Surviving sepsis campaign: International guidelines for management of sepsis and septic shock: 2016. *Critical Care Medicine*, 2017. URL <https://www.ncbi.nlm.nih.gov/pubmed/28101605>.

A Appendix

A.1 CVSim

CVSim is an open-source cardiovascular simulator, aiming for education and research purpose developed by Thomas et al[12]. In this work, we focus on CVSim-6C which consists of 6 components, functioning as pulmonary and systemic veins, arteries, and micro-circulations respectively. CVSim-6C is regulated by arterial baroreflex system to simulate Saha lumped hemodynamic model[12]. The aggregate model is capable of simulating pulsatile waveforms, cardiac output and venous return curves, and spontaneous beat-to-beat hemodynamic variability. In this work, we modified and built on CVSim by adding stochastic components to it for the purposes of evaluating our counterfactual simulators. We call our stochastic simulation engine S-CVSim.

A.2 Inputs of S-CVSim

By varying hemodynamic parameters of CVSim, it can simulate cardiovascular system under various conditions. We, therefore, sample values of a subset of model parameters while initiating simulation at time 0 to obtain ideal distribution of trajectories. These model parameters are listed at **Table 2**. **Note that this does not necessarily mean values of input covariates would not exceed or drop below such range at any time t , where $t > 0$.**

Table 2: Names and corresponding ranges of input parameters of S-CVSim.

INPUT COVARIATES	RANGE
Total Blood Volume	1,500 - 6,000
Nominal Heart Rate	40 - 160
Total Peripheral Resistance	0.1 - 1.4
Arterial Compliance	0.4 - 1.1
Pulmonary Arterial Compliance	0.1 - 19.9
Total Zero-pressure filling Volume	500 - 3,500
Pulmonary Arterial Compliance	2.0 - 3.4
Pulmonary Microcirculation Resistance	0.4 - 1.00

A.3 Outputs of S-CVSim

At each time t , CVSim-6C generates hemodynamic data including vascular resistance and varieties of type of flow, pressure, and volume. In addition to original 25 hemodynamic outputs, we introduce 3 new outputs, including **systolic blood pressure, diastolic blood pressure, and mean arterial pressure**, bringing the total number of output variables to 28. For this work, we only predict a subset of output covariates highlighted in **Table 3**. A complete list of

output are listed in **Table 3**.

- **Systolic Blood Pressure (SBP)** is defined as the highest measured arterial blood pressure while heart contracting.
- **Diastolic Blood Pressure (DBP)** is defined as the lowest measured arterial blood pressure while heart contracting.
- **Mean Arterial Pressure (MAP)** is defined as the average pressure in a patient's arteries during one cardiac cycle as follow formula. $MAP = \frac{2*DBP+1*SBP}{3}$

Table 3: Outputs of S-CVSim, L_t denotes all the output of S-CVSim at time t ; whereas, L_t^{any} denotes a subset of output e.g. L_t^{map} represents mean arterial pressure at time t . Covariates highlighted with * are the selected output.

OUTPUT COVARIATES	
Left Ventricle Pressure*	LVP
Left Ventricle Flow*	LVQ
Left Ventricle Volume	LVV
Left Ventricle Contractility*	LVC
Right Ventricle Pressure*	RVP
Right Ventricle Flow*	RVQ
Right Ventricle Volume	RVV
Right Ventricle Contractility*	RVC
Central Venous Pressure*	CVP
Central Venous Flow	CVQ
Central Venous Volume	CVV
Arterial Pressure*	AP
Arterial Flow*	AQ
Arterial Volume*	AV
Pulmonary Arterial Pressure	PAP
Pulmonary Arterial Flow	PAQ
Pulmonary Arterial Volume	PAV
Pulmonary Venous Pressure	PVP
Pulmonary Venous Flow	PVQ
Pulmonary Venous Volume*	PVV
Heart Rate*	HR
Arteriolar Resistance*	AR
Venous Tone*	VT
Total Blood Volume*	TBV
Intra-thoracic Pressure*	PTH
Mean Arterial Pressure*	MAP
Systolic Blood Pressure*	SBP
Diastolic Blood Pressure	DBP

A.4 Simulation Process

To obtain observational data for our intended purpose, we implemented and built two extra events, **Disease**, S_t and **Treatment**, A_t . Note that at each time T , both S_t and A_t could happen simultaneously but S_t also happens before A_t . With these stochastic events, A_t and S_t , D_{obs} and D_{CF}

can be simulated and obtained on S-CVSim.

A.4.1 Data Generation, D_o, D_c

To simulate a patient trajectory under treatment strategy g , we obtain D_o and D_c with the following algorithm for each individual trajectory. D_o , training set, consists of 10k trajectories based on g_o . D_c , test set, consists of 1k trajectories based on g_c .

- Initialize input variables V_1, \dots, V_N by drawing from independent uniform distributions using a predefined plausible physiological ranges for each variable as **Table 2** suggested.
- For t in $0:K$
 - Generate L_t^* as $F_{sim,t}(V, \bar{L}_{t-1}^*, A_{t-1})$, where A_{-1} is taken to be 0.
 - If $g = g_c$ and $t \geq \frac{K}{2}$:
 - * Generate A_t as $g_c(\bar{L}_t)$
 - Else
 - * Generate A_t as $g_o(\bar{L}_t)$

A.4.2 Disease Simulation, S_t

We introduce the concept S_t to simulate hemodynamic instability of cardiovascular system such as sepsis and bleeding at each timestep. S_t consists of two events, **sepsis** and **blood loss**. In module of S_t , we denote that $P(S_t|L_t) = 0.05$, and $P(Sepsis|S_t) = P(BloodLoss|S_t) = 0.5$; Note that blood loss and sepsis events are mutually exclusive in the simulation process at any time t .

- When sepsis happens, $L_{t+1}^{tpr} = \alpha_{tpr} * L_t^{tpr}$ where $0 < \alpha_{tpr} \leq 0.7$, meaning L_t^{tpr} , total peripheral resistance, would decrease in α_{tpr} at next time $t + 1$
- When blood loss happens, $L_{t+1}^{tbv} = \alpha_{tbv} * L_t^{tbv}$ where $0 < \alpha_{tbv} \leq 0.95$, meaning that L_t^{tbv} , total blood volume would decrease in α_{tbv} at next time $t + 1$.

A.4.3 Treatment Simulation, A_t

We developed two treatment strategy g_o , policy for observational regime and g_c , policy for counterfactual policy, to simulate clinical treatment and validate our model. Under any given g , A_t^{any} is defined as $g(L_t)$. Similar to disease simulation, A_t^{any} is either A_t^1 , **increasing quantity of total blood volume** or A_t^2 **increasing quantity of arterial resistance**. The probability of choosing fluids is equal to vasopressor but will not be administered at the same time. The dosage of A_t depends on a subset of L_t which indicates hemodynamic balance. More specific, since adequate blood pressure is an important clinical goal[26], we denote mean arterial pressure, MAP, of 65 mmHg and central venous pressure, CVP, of 10 mmHg as target goals. Therefore, We define $\Delta_{map,t} \equiv 65 - L_t^{map}$ and $\Delta_{cvp,t} \equiv 10 - L_t^{cvp}$ as proxies of how much dosage should be delivered. The fol-

lowing section will discuss the difference of A_t between g_{CF} and g_{obs} .

A.4.4 Observational Regime, g_o

Under g_{obs} , probability and dosage of treatment are denoted as the followings

- Probability of treatment, $P(A_t|L_t) = \frac{1}{1+e^{-x}}$, where $x = C_1 * \Delta_{map} + C_2 * \Delta_{cvp} + C_0$.
- If we administer fluids, we generate the dose (in mL) $A_t^1 \sim \max(0, \beta_1^1 * \Delta_{map,t} + \beta_2^1 * \Delta_{cvp,t} + \mathcal{N}(1500, 1000))$.
- If we administer vasopressors, we generate the dose $A_t^2 \sim \max(0, \beta_1^2 * \Delta_{map} + \beta_2^2 * \Delta_{cvp} + \mathcal{N}(0, 1))$ if $U \sim Uniform$.

A.4.5 Counterfactual Regime, g_c

Under g_{CF} , probability and dosage of treatment are denoted as the followings

- Probability of treatment, $P(A_t|L_t) = 1$ if and only if $L_t^{sbp} \leq 100$ and ShockIndex [26], $\frac{L_t^{hr}}{L_t^{sbp}}, \leq 0.8$.
- If we administer fluids, we generate the dose (in mL) $A_t^1 \sim \max(0, \beta_1^1 * \Delta_{map,t} + \beta_2^1 * \Delta_{cvp,t})$.
- If we administer vasopressors, we generate the dose $A_t^2 \sim \max(0, \beta_1^2 * \Delta_{map} + \beta_2^2 * \Delta_{cvp})$ if $U \sim Uniform$.

We experimented with multiple parameters and opted to use $C_0 = 0.02, C_1 = 0.06, C_2 = 0.24, \beta_1^1 = 10, \beta_2^1 = 60, \beta_1^2 = 0.1, \beta_2^2 = 0.15$.

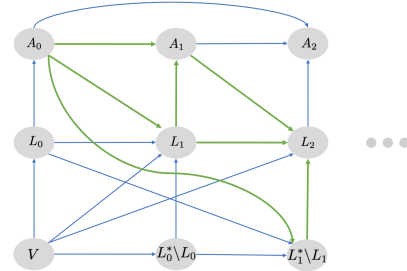


Figure 8: Causal DAG for D_o generated under observational regime g_o . Green arrows denote directed paths from treatments to outcomes. Treatment only depends on current covariates. All covariates with arrows into treatment (i.e. MAP, CVP, and Δ_P) are observed, satisfying the sequential exchangeability assumption as in Figure 1.

The DAG in Figure 8 depicts the causal structure of D_o . Note that only observed covariates have arrows pointing into treatment (treatment is actually only a function of CVP, MAP, and Δ_P), so that there is no unobserved confounding and g-computation may be applied.